Multiple Soft-Mode Vibrations of Lead Zirconate

J. Hlinka,* T. Ostapchuk, E. Buixaderas, C. Kadlec, P. Kuzel, I. Gregora, J. Kroupa, M. Savinov, A. Klic, and J. Drahokoupil
Institute of Physics, Academy of Sciences of the Czech Republic Na Slovance 2, 182 21 Prague 8, Czech Republic

I. Etxebarria
Zientzia eta Teknologia Fakultatea, Euskal Herriko Unibertsitatea, P.K. 644, 48080 Bilbao, Spain

J. Dec
Institute of Materials Science, University of Silesia, Bankowa 12, PL-40-007 Katowice, Poland
(Received 21 January 2014; published 12 May 2014)

Polarized Raman, IR, and time-domain THz spectroscopy of orthorhombic lead zirconate single crystals have yielded a comprehensive picture of temperature-dependent quasiharmonic frequencies of its low-frequency phonon modes. It is argued that these modes primarily involve vibrations of Pb ions and librations of oxygen octahedra. Their relation to phonon modes of the parent cubic phase is proposed. Counts of the observed IR and Raman active modes belonging to distinct irreducible representations agree quite well with group-theory predictions. Analysis of the results yields insight into the phase transition mechanism, involving a soft ferroelectric branch coupled by a trilinear term to another two oxygen octahedra tilt modes.

DOI: 10.1103/PhysRevLett.112.197601 PACS numbers: 77.80.-e, 63.20.D-, 77.84.Cg

Reexamination of the antiferroelectricity in $PbZrO_3$ [1–4] resulted in the renouncement of the original simple two-sublattice Kittel model [5], at least in the case of this canonical antiferroelectric (AFE) oxide. Most recent studies suggest that the AFE state in lead zirconate is induced by a single lattice mode—the ferroelectric (FE) soft mode—through its flexoelectric [6–10] interaction with antiphase lead displacements [4]. The oxygen octahedra tilt displacements are triggered [11] by a biquadratic interaction to the antiphase lead displacements [4]. This novel approach to the antiferroelectricity in $PbZrO_3$ raises many questions not only with respect to this single compound and its widespread derivatives [12–16], but also with respect to interfacial engineering [17,18], design strategy of new antiferroelectrics, and their new application perspectives as well [1,2,19].

Here we describe a detailed polarized IR and Raman spectroscopic study of single domain specimens of AFE $PbZrO_3$. The obtained results demonstrate the existence of multiple soft modes of different symmetry. From their analysis an alternative model has emerged, in which (i) the whole phonon branch related to lead vibrations is intrinsically soft, and (ii) the AFE state is directly stabilized by a trilinear coupling term, that drives the AFE lead displacements and the oxygen octahedra tilts simultaneously.

The paraelectric (PE) phase of $PbZrO_3$ is a simple cubic perovskite with a 5-atom unit cell ($Pm\bar{3}m$, $Z = 1$). Below the AFE phase transition ($T_C \sim 500$ K), it goes over to an orthorhombic $Pbam$ ($Z = 8$) structure [20,21]. The space-group symmetry change can be well understood [2] as a result of the condensation of 2 order parameters [2,4,17,21–23]: a polarization wave of a propagation vector $\mathbf{Q}_\Sigma = (0.25, 0.25, 0)_{\mathrm{pc}}$ and a $\mathbf{Q}_R = (0.5, 0.5, 0.5)_{\mathrm{pc}}$ oxygen octahedra tilt mode (here pc stands for pseudocubic lattice, see Figs. 1 and 2). Superpositions of $\mathbf{Q}_\Sigma$, $\mathbf{Q}_R$ include also Γ, X, M, and $\mathbf{Q}_S = (0.25, 0.25, 0.5)_{\mathrm{pc}}$ cubic-phase Brillouin zone points. All of these points become Brillouin zone centers in the $Pbam$ phase [see Fig. 2(a)] and the corresponding lattice modes give rise to $16A_g + 16B_{1g} + 14B_{2g} + 14B_{3g} + 12A_u + 11B_{1u} + 17B_{2u} + 17B_{3u}$ optic modes of the $Pbam$ structure. In the AFE phase, the optical spectroscopy thus effectively allows probing phonon modes from the Σ and S lines.

Density functional theory calculations demonstrated that the cubic structure of $PbZrO_3$ is instable at low temperatures with respect to the Pb ion off centering as well as concerted oxygen octahedra tilts [3,23,25–27,31]. The corresponding finite-temperature phonon frequencies can be estimated from the inelastic neutron and x-ray scattering studies $PbTiO_3$-$PbZrO_3$ solid solutions (PZT) in their common cubic phase. For example, the frequencies of the M_5', M_2', X_5', X_2', and R_{15} Pb-dominated modes can be extrapolated from the measurements of the $PbTiO_3$ [28–30] and the PZT single crystals [32]. The acoustic mode dispersion can be estimated from $PbZrO_3$ measurements of Refs. [4,33,34], and the zone-center mode frequency can be estimated from the dielectric measurements [4,35,36]. The lowest frequency phonon dispersion curves of the cubic $PbZrO_3$ obtained in this way (near the phase transition point) are traced in Fig. 2(b).

In the limit of vanishing structural distortion (small order parameters), Γ-point modes of the $Pbam$ orthorhombic

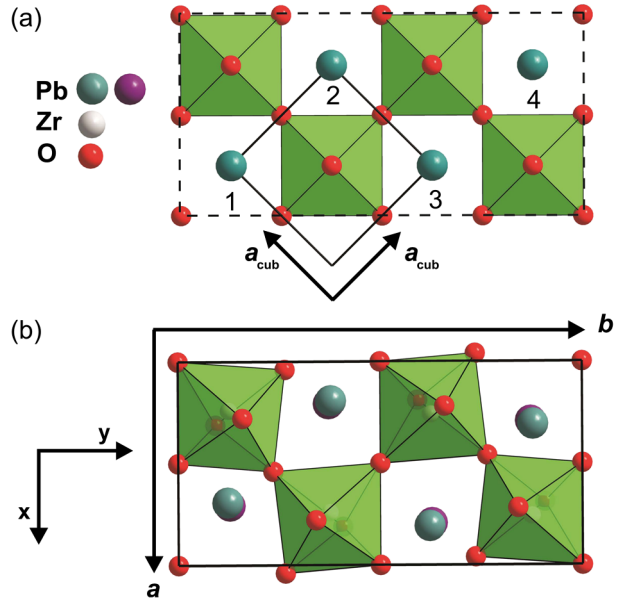

FIG. 1 (color online). Crystal structure of $PbZrO_3$ in its (a) high-temperature cubic phase and (b) in its low-temperature orthorhombic phase. The orthorhombic *Pbam* elementary unit cell is projected along its $z \| \mathbf{c}$ axis, the $\mathbf{a} = (1, -1, 0)_{pc}/\sqrt{2}$ and $\mathbf{b} = (1, 1, 0)_{pc}\sqrt{2}$ lattice vectors defining the x and y axes are indicated in the figure. Note that the x components of the AFE displacements of the Pb ions 1 and 2 are opposite to those of 3 and 4. This displacement pattern forms a Σ_3 symmetry mode associated with $\mathbf{Q}_\Sigma = \mathbf{b}^*$ propagating vector.

structure transform also as $\Gamma, X, R, M, \mathbf{Q}_\Sigma$ or $\mathbf{Q}_S$-point modes of the parent cubic phase. Correlation between irreducible representations of the actual and parent symmetry group for the Pb ion vibration modes is shown in Table I. The items listed in Table I match well the cubic-phase modes shown in Fig. 2(b). Therefore, about 24 optic Pb ion modes are expected in the AFE phase within the 0–100 cm^{-1} frequency range.

To identify these modes experimentally, we have investigated flux-grown single crystal platelets detwinned using

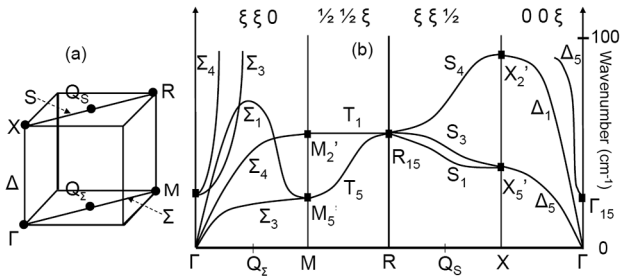

FIG. 2. Brillouin zone points involved in the phase transition and low-frequency phonon branches of cubic $PbZrO_3$. Panel (a) indicates $\Gamma, X, R, M, \mathbf{Q}_\Sigma$ and $\mathbf{Q}_S$ Brillouin zone points of cubic $PbZrO_3$; panel (b) shows corresponding phonon frequencies estimated from the available $PbTiO_3$ and $PbTiO_3$-$PbZrO_3$ spectroscopic data. Indices of the symmetry labels denoting phonon branches are those of Ref. [24].

the method of Ref. [37], with either out-of-plane or in-plane c axis [37]. Raman data were collected using a Renishaw microscope spectrometer operated with a 514 nm laser and a low-frequency edge filter, like, e.g., in Refs. [38,39]. IR reflectivity and time-domain THz transmission data were collected using a Fourier-transform Bruker spectrometer and a laboratory built system based on a Ti-sapphire laser, respectively, and then fitted simultaneously to obtain consistent complex dielectric and conductivity spectra in the 10–800 cm^{-1} range (the same setup and experimental procedure as, e.g., in Refs. [40,41]).

The typical low-frequency, low-temperature Raman spectra are shown in Figs. 3(a) and 3(b). As indicated in the figure, the light was polarized along the *Pbam* crystallographic axes so that the assignment of the observed modes to the relevant irreducible representations was rather straightforward. Similarly, the real part of the conductivity spectra allows probing the $B_{1u}(z), B_{2u}(y)$, and $B_{3u}(x)$ modes independently [see Fig. 3(c)]. Therefore, present data offered a more complete picture than the earlier studies [42–44]. Overall, the numbers of the modes observed in the 0–100 cm^{-1} frequency range match well the list given in Table I.

Phonon frequencies up to about 150 cm^{-1} (from fits using damped harmonic oscillator response functions) as a function of temperature are shown in Fig. 4. The lowest frequency B_{2u}, B_{3u}, B_{1g}, and B_{2g} modes can be assigned to the $\Sigma_3, \Sigma_1, \Sigma_1$, and Σ_4 acoustic modes folded from $(\mathbf{Q}_\Sigma)$. All other modes of Fig. 4 reveal a considerable *frequency increase upon cooling* (both the modes in the 0–100 cm^{-1} range as well as those in the 100–150 cm^{-1} frequency range). How can this be understood?

The temperature dependence of the fully symmetric mode (A_g), corresponding to the order parameter, follows naturally from the simplest Landau-type theory. The temperature dependence of the B_{1u}, B_{2u}, and B_{3u} components of the Last-type Γ_{15} mode could be, in principle, explained, e.g., by a positive biquadratic coupling to the primary order parameter [4]. However, the simplest assumption explaining the strikingly similar temperature dependence of so many *other* phonon frequencies below 100 cm^{-1} is that $PbZrO_3$ has a soft branch, rather than a

TABLE I. Correlation between D_{2h} irreducible representations of *Pbam* Pb-ion zone-center vibrations (top row of the table) and their counterparts in the parent cubic phase. Σ_i and S_i stands for modes associated with $\mathbf{Q}_\Sigma$ and $\mathbf{Q}_S$ wave vectors, respectively. Other labels are as those of Ref. [31].

	A_g	$B_{1g}(xy)$	$B_{2g}(xz)$	$B_{3g}(zy)$	A_u	$B_{1u}(z)$	$B_{2u}(y)$	$B_{3u}(x)$
Γ						Γ_{15}	Γ_{15}	Γ_{15}
X						X_2'	X_5'	X_5'
M	M_5'	M_5'		M_2'				
R	R_{15}	R_{15}		R_{15}				
Σ	Σ_3	Σ_1	Σ_4		Σ_4		Σ_3	Σ_1
S	S_3	S_1	S_4		S_4		S_3	S_1

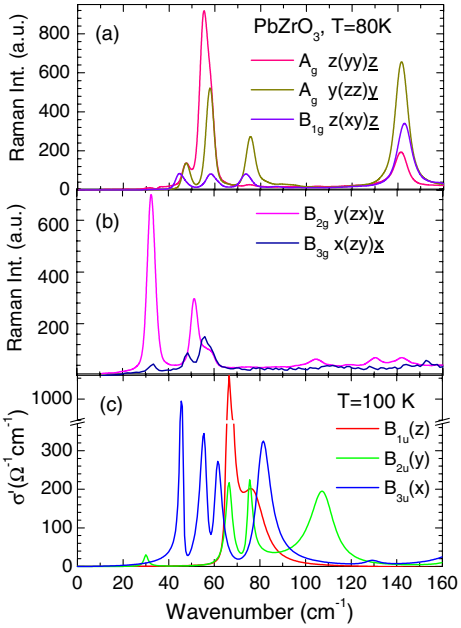

FIG. 3 (color online). Typical low-frequency phonon spectra of $PbZrO_3$. Panels (a) and (b) shows polarized Raman spectra at 80 K. The scattering geometry is indicated using standard Porto notation. Panel (c) shows the real part of the low-frequency conductivity spectra, as obtained from a combined fit to the spectra of IR reflectivity and time-domain THz spectroscopy, showing peaks at the transverse optic mode frequencies of the $B_{1u}(z)$, $B_{2u}(y)$, and $B_{3u}(x)$ modes. The x, y, and z labels correspond to the crystallographic axes of the orthorhombic *Pbam* structure.

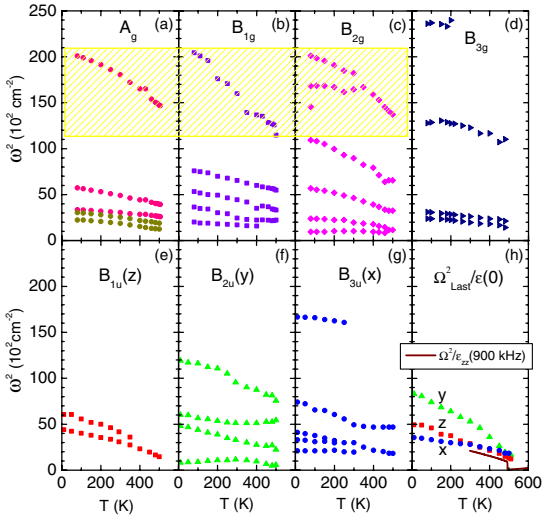

FIG. 4 (color online). Temperature dependence of squared frequencies of Raman active (a)–(d) and IR active (e)–(g) modes of AFE $PbZrO_3$. Panel (h) shows inverse static permittivity multiplied by the square of the plasma frequency of the Last mode ($\Omega_{\text{Last}} = 618$ cm^{-1}). It provides an estimate of the squared oscillator frequency of the bare Last mode. Values of $\epsilon(0)$ are taken from the joint THz-IR fit (point symbols). Independently measured 900 kHz data (available only along the c axis) are shown by the continuous line. The yellow-shaded region indicates soft oxygen octahedra libration modes.

single soft-mode driven phase transition. Soft branches are known, e.g., from incommensurate dielectrics [44–47]. Actually, present results even suggest that both Σ_3 and S_3 branches are temperature dependent here.

Obviously, among the modes of the same irreducible representation, the temperature dependence can be shared due to the mode mixing. In particular, modes listed within the same column in Table I are coupled in the AFE phase. For example, we have verified that the overall IR plasma frequency [48] of all B_{3u} modes observed below 100 cm^{-1} is close to the IR plasma frequency of the Last soft mode $\Omega_{\text{Last}} = 618$ cm^{-1} determined from the analysis of the cubic phase spectra [48]. Since the bare X_5', Σ_1, and S_1 modes have the B_{3u} symmetry but no intrinsic IR strength, the relative integral intensities of the B_{3u} modes observed in the conductivity spectrum below 100 cm^{-1} [Fig. 3(c)] can be directly interpreted as a measure of their eigenvector exchange with the pure Last mode [48]. This mixing is quite considerable.

Are the observed temperature variations of phonon frequencies large or small? Within the Landau theory of the second-order structural phase transition, the squared soft-phonon frequency shows a linear temperature dependence (Cochran law). A stronger, *nonlinear* temperature dependence is expected below a first-order phase transition point, but the relation of the inverse static permittivity to the soft-mode frequency via the Lyddane-Sachs-Teller relation should be still valid. To estimate the expected soft-mode frequency, we have thus multiplied the inverse of the static limit of the fitted permittivity by the square of the mode plasma frequency of the Last mode (Ω_{Last}), and traced the resulting squared bare Last mode frequency [$\omega^2_{\text{Last, i}} = \Omega^2_{\text{Last}}/\epsilon_i(0)$, $i = x, y, z$] in Fig. 4(h). Indeed, such bare mode frequencies show very similar temperature dependence as most of the directly measured mode frequencies below 100 cm^{-1}.

Let us stress that the A_g, B_{1g}, and B_{2g} Raman spectra show a second family of soft modes, with frequencies above 100 cm^{-1}, and an even stronger temperature dependence (Fig. 4). These modes correspond well to the soft mode reported in Refs. [42,43]. It is natural to ascribe them to descendants of the R_{25} rigid oxygen octahedra tilt mode, known as the soft mode of the structural phase transition of $SrTiO_3$ crystal [24]. Indeed, the R_{25} mode components associated with oxygen octahedra tilts around the x, y, and z orthorhombic axes do transform precisely as the A_g, B_{1g}, and B_{2g} irreducible representations.

From these results, a new understanding emerges. A pronounced temperature dependence of the BZ center soft mode is well known from several FE materials [Fig. 5(a)]; hence, by a simple analogy one could expect a soft zone-boundary mode in the case of an AFE material [Fig. 5(b)]. However, no such case is known. In fact, in a good AFE

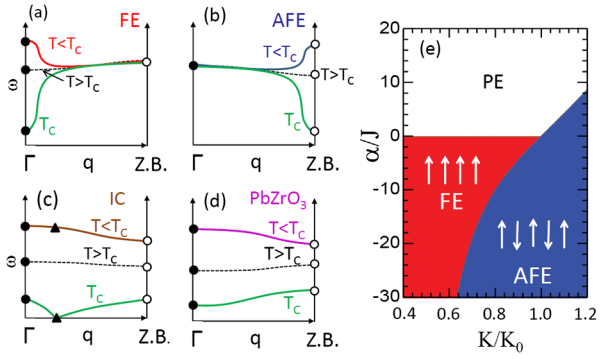

FIG. 5 (color online). Different kinds of soft-mode driven phase transitions. Panels (a)–(d) show schematically phonon dispersion of the polarization branch at $T > T_C$, $T \approx T_C$, and $T < T_C$ (traced in the parent-phase Brillouin zone) for a typical FE phase transition (a), hypothetical AFE phase transition (b), incommensurate transition (c), and in $PbZrO_3$, as inferred from the present study (d). Panel (e) shows a phase diagram of the model described by Eqs. (1)–(2) with $\beta = 1$, $B = 1$, $J = 0.1$, $A = 1$ [49].

material, one should be also able to switch the staggered polarization configuration to the FE one by an electric field. This suggests that AFE materials should have both the zone-center and zone-boundary soft mode. It is most naturally realized when the whole polarization branch is soft [Fig. 5(c)]. This often results in an incommensurate instability [45–47]. A combination of the present experimental results and those of Ref. [4] implies that $PbZrO_3$ does exhibit a flat soft polarization branch, still without any trace of a local minimum near the AFE wave vector [Fig. 5(d)]. Therefore, an additional ingredient responsible for the antiferroelectricity is needed beyond the quasiharmonic approximation, i.e., a nonlinear coupling term. The existence of the second family of soft modes (range 100–150 cm^{-1}) suggests that this term involves the oxygen octahedra tilts.

To illustrate this idea, we consider a 1D chain of alternating lead and oxygen ions in the direction of the AFE wave vector, e.g., all ions located on the line connecting (1) and (3) Pb ions shown in Fig. 1. A simple soft branch potential related to x displacement of nth lead ion p_n reads

$$\sum \left[\frac{\alpha}{2} p_n^2 + \frac{\beta}{4} p_n^4 + \frac{J}{2} (p_{n+1} - p_n)^2 \right], \tag{1}$$

with $\alpha = a(T - T_0)$, $a, \beta, J > 0$. Note that the usual Landau term $\alpha/2(\sum p_n)^2$ for the soft macroscopic polarization is replaced with an effective-Hamiltonian-like [23,25] $\alpha/2 \sum p_n^2$ expression describing the soft microscopic polarization. Therefore, this term directly controls the stability of both AFE and FE modes. The second ingredient is a potential associated with x and y displacements of the nth oxygen ion x_n, y_n and a coupling term to adjacent Pb ions that favors their AFE arrangement, such as

$$\sum \left[\frac{A}{2} (x_n^2 + y_n^2) + \frac{B}{4} (x_n^4 + y_n^4) + \frac{K}{2} (p_{n+1} - p_n) x_n y_n \right], \tag{2}$$

with $A, B > 0$. The phase diagram of this model is sketched in Fig. 5(e). The direct paraelectric ($p_n = 0$) to AFE [$p_n = p(-1)^n$] phase transition occurs if $|K| > K_0 \doteq 0.9425$. For a smaller magnitude of K, the AFE transition is preceded by the FE one ($p_n = p$), as in the Zr-rich side of the temperature-concentration phase diagram of the PZT system. Similar phase diagrams can be expected to hold for a more realistic, 3D lattice model with all the trilinear coupling terms allowed by symmetry, such as that involving the product of the Σ_3 polarization wave with R_{25} and S_3 octahedra rotation modes [49]. In this sense the AFE phase transition of $PbZrO_3$ is analogical to the avalanche [50–52] and "hybrid-improper-like" [53] transitions.

In summary, this polarized Raman, IR, and THz spectroscopic study of AFE $PbZrO_3$ single crystals has established that there are several low frequency modes with anomalously temperature dependent phonon frequencies distributed among seven active irreducible representations. We conclude that the modes around 130 cm^{-1} are associated with oxygen octahedra tilt vibrations, while those below about 100 cm^{-1} are due to the Pb ion fluctuations. Softening of the latter can be understood as a consequence of a soft and flat phonon branch, without having to recall specific biquadratic couplings for each such mode separately. It is emphasized that, in general, flat soft polarization branches ensure a simultaneous instability with respect to both the homogeneous and the staggered polarization, that seems to be the essential prerequisite of an AFE material [54,55]. Switching is actually easier when the AFE instability is weaker than the FE one. However, this situation requires an additional element stabilizing the staggered polarization, such as the above proposed trilinear term for $PbZrO_3$. We hope that this piece of understanding can help to discover new useful antiferroelectrics as well as to model the finite-temperature properties of the current $PbZrO_3$-based materials.

The authors are indebted to J. Petzelt for a critical reading of the manuscript. The work was supported by the Czech Science Foundation (Project No. GACR 13-15110S).

*hlinka@fzu.cz

[1] H. Liu and B. Dkhil, Z. Kristallogr. **226**, 163 (2011).
[2] K. M. Rabe, in *Functional Metal Oxides: New Science and Novel Applications*, edited by Satish Ogale and V. Venkateshan (Wiley, Hoboken, NJ, 2013).
[3] S. E. Reyes-Lillo and K. M. Rabe, Phys. Rev. B **88**, 180102 (2013).
[4] A. K. Tagantsev, K. Vaideeswaran, S. B. Vakhrushev, A. V. Filimonov, R. G. Burkovsky, A. Shaganov, D. Andronikova, A. I. Rudskoy, A. Q. R. Baron, H. Uchiyama, D. Chernyshov,

A. Bosak, Z. Ujma, K. Roleder, A. Majchrowski, J.-H. Ko, and N. Setter, Nat. Commun. **4**, 2229 (2013).
[5] C. Kittel, Phys. Rev. **82**, 729 (1951).
[6] P. Zubko, G. Catalan, and A. K. Tagantsev, Annu. Rev. Mater. Res. **43**, 387 (2013).
[7] A. K. Tagantsev, Phys. Rev. B **34**, 5883 (1986).
[8] J. Hong and D. Vanderbilt, Phys. Rev. B **88**, 174107 (2013).
[9] M. Stengel, Phys. Rev. B **88**, 174106 (2013).
[10] P. V. Yudin and A. K. Tagantsev, Nanotechnology **24**, 432001 (2013).
[11] J. Holakovsky, Phys. Status Solidi B **56**, 615 (1973).
[12] M. E. Lines and A. M. Glass, *Principles and Applications of Ferroelectrics and Related Materials* (Oxford University Press, New York, 1977).
[13] G. Shirane, E. Sawaguchi, and A. Takeda, Phys. Rev. **80**, 482 (1950).
[14] A. S. Bhala, R. Guo, and R. Roy, Mater. Res. Innovations **4**, 3 (2000).
[15] B. Jaffe, W. R. Cook, and H. Jaffe, *Piezoelectric Ceramics* (Academic Press, London, 1971).
[16] I. A. Kornev, L. Bellaiche, P.-E. Janolin, B. Dkhil, and E. Suard, Phys. Rev. Lett. **97**, 157601 (2006).
[17] X. K. Wei, A. K. Tagantsev, A. Kvasov, K. Roleder, C. L. Jia, and N. Setter, Nat. Commun. **5**, 3031 (2014).
[18] A. R. Chaudhuri, M. Arredondo, A. Hahnel, A. Morelli, M. Becher, M. Alexe, and I. Vrejoiu, Phys. Rev. B **84**, 054112 (2011).
[19] A. S. Mischenko, Q. Zhang, J. F. Scott, R. W. Whatmore, and N. D. Mathur, Science **311**, 1270 (2006).
[20] A. M. Glazer, K. Roleder, and J. Dec, Acta Crystallogr. Sect. B **49**, 846 (1993).
[21] H. Fujishita and S. Hoshino, J. Phys. Soc. Jpn. **53**, 226 (1984).
[22] H. Fujishita, Y. Shiozaki, N. Achiwa, and E. Sawaguchi, J. Phys. Soc. Jpn. **51**, 3583 (1982).
[23] U. V. Waghmare and K. M. Rabe, Ferroelectrics **194**, 135 (1997).
[24] R. A. Cowley, Phys. Rev. **134**, A981 (1964).
[25] E. Cockayne and K. M. Rabe, J. Phys. Chem. Solids **61**, 305 (2000).
[26] K. Leung, E. Cockayne, and A. F. Wright, Phys. Rev. B **65**, 214111 (2002).
[27] K. Leung, Phys. Rev. B **67**, 104108 (2003).
[28] G. Shirane, J. D. Axe, J. Harada, and J. P. Remeika, Phys. Rev. B **2**, 155 (1970).
[29] I. Tomeno, J. A. Fernandez-Baca, K. J. Marty, K. Oka, and Y. Tsunoda, Phys. Rev. B **86**, 134306 (2012).
[30] M. Kempa, J. Hlinka, J. Kulda, P. Bourges, A. Kania, and J. Petzelt, Phase Transit. **79**, 351 (2006).
[31] Ph. Ghosez, E. Cockayne, U. V. Waghmare, and K. M. Rabe, Phys. Rev. B **60**, 836 (1999).
[32] J. Hlinka, P. Ondrejkovic, M. Kempa, E. Borissenko, M. Krisch, X. Long, and Z.-G. Ye, Phys. Rev. B **83**, 140101 (2011).
[33] J.-H. Ko, M. Górny, A. Majchrowski, K. Roleder, and A. Bussmann-Holder, Phys. Rev. B **87**, 184110 (2013).
[34] F. Cordero, F. Craciun, and C. Galassi, Phys. Rev. Lett. **98**, 255701 (2007).
[35] E. Buixaderas, D. Nuzhnyy, J. Petzelt, L. Jin, and D. Damjanovic, Phys. Rev. B **84**, 184302 (2011).
[36] T. Ostapchuk, J. Petzelt, V. Zelezny, S. Kamba, V. Bovtun, V. Porokhonskyy, A. Pashkin, P. Kuzel, M. D. Glinchuk, I. P. Bykov, B. Gorshunov, and M. Dressel, J. Phys. Condens. Matter **13**, 2677 (2001).
[37] J. Dec and J. Kwapulinski, J. Phys. Condens. Matter **1**, 3389 (1989).
[38] J. Hlinka, I. Gregora, J. Pokorny, C. Hérold, N. Emery, J. F. Mareché, and P. Lagrange, Phys. Rev. B **76**, 144512 (2007).
[39] F. Borodavka, I. Gregora, A. Bartasyte, S. Margueron, V. Plausinaitiene, A. Abrutis, and J. Hlinka, J. Appl. Phys. **113**, 187216 (2013).
[40] J. Hlinka, T. Ostapchuk, D. Nuzhnyy, J. Petzelt, P. Kuzel, C. Kadlec, P. Vanek, I. Ponomareva, and L. Bellaiche, Phys. Rev. Lett. **101**, 167402 (2008).
[41] D. Nuzhnyy, J. Petzelt, M. Savinov, T. Ostapchuk, V. Bovtun, M. Kempa, J. Hlinka, V. Buscaglia, M. T. Buscaglia, and P. Nanni, Phys. Rev. B **86**, 014106 (2012).
[42] P. S. Dobal, R. S. Katiyar, S. S. N. Bharadwaja, and S. B. Krupanidhi, Appl. Phys. Lett. **78**, 1730 (2001).
[43] K. Roleder, G. E. Kugel, M. D. Fontana, J. Handerek, S. Lahlou, and C. Carabatos-Nedelec, J. Phys. Condens. Matter **1**, 2257 (1989).
[44] J. Hlinka, O. Hernandez, M. Quilichini, and R. Currat, Ferroelectrics **185**, 221 (1996).
[45] J. Hlinka, M. Quilichini, R. Currat, and J.-F. Legrand, J. Phys. Condens. Matter **8**, 8207 (1996).
[46] J. Hlinka, M. Quilichini, R. Currat, and J.-F. Legrand, J. Phys. Condens. Matter **8**, 8221 (1996).
[47] I. Etxebarria, M. Quilichini, J. M. Perez-Mato, P. Boutrouille, F. J. Zuniga, and T. Breczewski, J. Phys. Condens. Matter **4**, 8551 (1992).
[48] J. Hlinka, J. Petzelt, S. Kamba, D. Noujni, and T. Ostapchuk, Phase Transit. **79**, 41 (2006).
[49] See Supplemental Material at http://link.aps.org/supplemental/10.1103/PhysRevLett.112.197601 for computational details.
[50] I. Etxebarria, J. M. Perez-Mato, and P. Boullay, Ferroelectrics **401**, 17 (2010).
[51] J. M. Perez-Mato, M. Aroyo, A. Garcia, P. Blaha, K. Schwarz, J. Schweifer, and K. Parlinski, Phys. Rev. B **70**, 214111 (2004).
[52] U. Petralanda and I. Etxebarria, Phys. Rev. B **89**, 064107 (2014).
[53] A. T. Mulder, N. A. Benedek, J. M. Rondinelli, and C. J. Fennie, Adv. Funct. Mater. **23**, 4810 (2013).
[54] V. Dvorak, Phys. Status Solidi **14**, K161 (1966).
[55] G. A. Samara, Phys. Rev. B **1**, 3777 (1970).